

Synchrotron-betatron resonances in free-electron lasers

W. M. Fawley, D. Prosnitz, and E. T. Scharlemann

Lawrence Livermore National Laboratory, University of California, P.O. Box 808, Livermore, California 94550

(Received 4 June 1984)

The coupling between betatron and synchrotron oscillations in a tapered wiggler free-electron laser (FEL) is investigated analytically and numerically. The resonance between the oscillations, first investigated by Rosenbluth, is shown to be important only for a very limited range of parameters. In general, the resonance is not a serious detrapping mechanism for high-power FEL amplifiers.

I. INTRODUCTION

Tapered wiggler free-electron lasers¹ have been proposed as efficient, high-power sources for various purposes (e.g., inertial confinement fusion). These devices will work as intended only if those electrons which are trapped in ponderomotive potential wells can be adiabatically decelerated. The electron energy lost in the deceleration is gained by the electromagnetic field. Any effect which permits trapped electrons to escape the potential wells during deceleration decreases the fraction of electron-beam energy that can be converted to radiation.

Rosenbluth² has suggested that resonance between the synchrotron and betatron oscillations of an electron can be such a detrapping effect. Synchrotron oscillations are the quasiperiodic motions of an electron trapped in a ponderomotive potential well.¹ Betatron oscillations are the harmonic motion in the x - y plane (transverse to the beam and laser-propagation direction) and are due to the transverse variations of the wiggler magnetic field strength, and to external focusing (if any; see Sec. VI). The oscillations are coupled if the wavefronts of the laser field are curved; the betatron motion then periodically forces the electron to different phases in the ponderomotive potential well. The electron's natural synchrotron oscillations can become amplified when they and the betatron forcing are in approximate resonance.

Rosenbluth showed that the range in laser power for which resonance occurs partly overlaps that proposed for high-power free-electron-laser (FEL) amplifiers. In order to assess the importance of resonant detrapping, we have extended Rosenbluth's analysis with a numerical study of the resonance, and with two-dimensional particle simulations of its effects in high-power amplifiers. We find quite generally that the adverse effects of resonant detrapping are greatly ameliorated by two other effects: First, high gain combined with the wiggler taper moves the electrons through resonance too rapidly for many to be detrapped, and, second, gain rapidly straightens the wavefronts of the laser field, thereby decreasing the coupling between betatron and synchrotron motions. We conclude that resonant detrapping critically affects FEL operation only if it is designed to.

This paper is organized in the following manner. In Sec. II we rederive the resonance equations in the labora-

tory frame; Rosenbluth's approximations are elucidated. In Sec. III we describe a numerical study of the resonance equations and the critical boundaries in parameter space within which synchrotron-betatron resonance detraps electrons. In Sec. IV we describe the simulation code in some detail, and in Sec. V we substantiate the conclusions mentioned in the preceding paragraph. In Sec. VI we briefly discuss an alternative origin for detrapping by synchrotron-betatron resonance; the presence of strong external (nonwiggler) focusing may produce another form of the resonance which can easily dominate that due to phase-front curvature.

II. RESONANCE EQUATIONS

Rosenbluth² worked with the electron equations of motion in a frame of reference moving with the ponderomotive potential well. We prefer to work in the laboratory (wiggler) frame, but the connection with the ponderomotive frame can be made without difficulty.

In the absence of external focusing, an electron in a helical wiggler executes approximately harmonic betatron motion in both transverse dimensions x and y :

$$\frac{d^2}{dz^2}(x,y) = -k_\beta^2(x,y), \quad (1)$$

where

$$k_\beta = \frac{ek_w A_w}{\sqrt{2}\gamma mc} \equiv \frac{b_w}{\sqrt{2}\gamma} \quad (\text{SI units}). \quad (2)$$

A_w is the wiggler magnetic vector potential,

$$A = A_w \left[\hat{x} \left[1 + \frac{k_w^2 y^2}{2} \right] \sin(k_w z) + \hat{y} \left[1 + \frac{k_w^2 x^2}{2} \right] \cos(k_w z) \right], \quad (3)$$

and γ is the Lorentz factor of the electron. This form [Eq. (3)] for the wiggler field is an approximation to a "realizable" wiggler field,³ it satisfies Maxwell's equations through $O(k_w^2 r^2)$, and thus is a good approximation for small betatron amplitudes.

The electric field of the laser radiation that is amplified by electron motion in the wiggler of Eq. (3) is circularly

polarized, and can be written as

$$E = \text{Re}[E_s(\hat{x} + i\hat{y})e^{i(k_s z - \omega_s t) + i\varphi}] . \quad (4)$$

Both E_s and φ are functions of x , y , and z .

The longitudinal equations of motion for an electron in the combined wiggler and laser field are most conveniently written in the variables γ and ψ (the phase of the electron in the ponderomotive potential well):⁴

$$\frac{d\psi}{dz} = k_w - \frac{k_s}{2\gamma^2}(1 + a_w^2 + \gamma^2\beta_1^2 - 2a_w a_s \cos\psi) + \frac{d\varphi}{dz} , \quad (5)$$

$$\frac{d\gamma}{dz} = -\frac{a_w e_s}{\gamma} \sin\psi . \quad (6)$$

Here, $a_s \equiv e_s/k_s = eE_s/k_s mc^2$, and $a_w \equiv b_w/k_w$. Equation (5) is correct to first order in a_s , invariably a small dimensionless number, and assumes that $\gamma^2 \gg 1 + a_w^2$.

The $\gamma^2\beta_1^2$ term in Eq. (5) is the square of the electron's dimensionless x - y momentum in its betatron orbit. When the betatron motion is due entirely to helical wiggler focusing [Eqs. (1) and (2)], the sum $a_w^2 + \gamma^2\beta_1^2$ remains constant throughout the betatron motion of an individual electron.

The coupling discussed by Rosenbluth² between betatron (x - y) motion and synchrotron (γ - ψ) motion occurs via the $d\varphi/dz$ term of Eq. (5). If φ depends on x or y (i.e., if the phase fronts of the laser field are curved), then the betatron motion produces a periodic forcing term in the expression for $d\psi/dz$.

For a vacuum Gaussian laser beam,

$$e_s(r, z, t) = e_0 \left[\frac{w_0}{w} \right] e^{-r^2/w^2} e^{i(k_s z - \omega_s t) + i\varphi} , \quad (7)$$

with φ and w expressible as

$$\varphi(r, z) = \varphi(0, z) + \frac{k_s r^2}{2R} , \quad (8)$$

$$w = w_0 \left[1 + \left(\frac{z}{z_R} \right)^2 \right]^{1/2} . \quad (9)$$

The radius of curvature (R) of the phase fronts is given by

$$R = z \left[1 + \left(\frac{z_R}{z} \right)^2 \right] , \quad (10)$$

where z is measured from the longitudinal position of the laser-beam waist. Here, $z_R = k_s w_0^2/2$ is the Rayleigh length; w_0 is the radius at the beam waist, at $z=0$. The phase on axis, $\varphi(0, z) = -\tan^{-1}(z/z_R)$, is slowly varying and can be neglected in Eq. (5).

Individual electrons follow elliptical orbits in the wiggler field of Eq. (3). Those in circular orbits are not affected by phase-front curvature because r (hence φ) is constant in Eq. (8). Those in linear orbits are affected most; r varies from 0 to a maximum, r_β . We will consider primarily electrons in linear orbits in this section (although the simulations described in Sec. V include orbits of arbitrary eccentricity).

For an electron in a linear orbit,

$$r = r_\beta \cos(k_\beta z + \varphi_\beta) , \quad (11)$$

where φ_β is an arbitrary initial betatron phase. If the radius of curvature of the phase fronts and the beam size change slightly over several betatron periods, Eqs. (5) and (6) yield a second-order equation for ψ :

$$\begin{aligned} \frac{d^2\psi}{dz^2} = & -\frac{a_w e_s}{\gamma^2} \left[k_w + \frac{k_s}{2\gamma^2}(1 + a_w^2 + \gamma^2\beta_1^2) \right] \sin\psi \\ & - \frac{k_s k_\beta^2 r_\beta^2}{R} \cos[2(k_\beta z + \varphi_\beta)] - \frac{k_s}{2\gamma^2} \frac{d}{dz}(a_w^2 + \gamma^2\beta_1^2) . \end{aligned} \quad (12)$$

Here we have assumed that $a_s k_s / 2\gamma k_w \ll 1$, permitting us to drop several terms that are negligible in that limit. The term proportional to $d(a_w^2 + \gamma^2\beta_1^2)/dz$ vanishes when the betatron motion is described by Eqs. (1) and (2); it can be important if there is other external focusing of the electron beam. We defer discussion of that term until Sec. VI, and for now assume it to vanish.

If we assume that both (a) the sum $a_w^2 + \gamma^2\beta_1^2$ is constant, and (b) γ is constant and equal to the synchronous energy¹ γ_r (for which $d\psi/dz = 0$ in the absence of phase front curvature), where

$$\gamma_r^2 \equiv \frac{k_s}{2k_w}(1 + a_w^2 + \gamma^2\beta_1^2) , \quad (13)$$

the usual pendulum equation,⁵ with the addition of a periodic forcing term, is recovered:

$$\frac{d^2\psi}{dz^2} = -\frac{2e_s b_w}{\gamma_r^2} \sin\psi - \frac{k_s k_\beta^2 r_\beta^2}{R} \cos[2(k_\beta z + \varphi_\beta)] . \quad (14)$$

Equation (14) can be made dimensionless by introducing

$$\Omega_s^2 = e^{-\lambda} \left[\frac{w_0}{w} \right] \frac{2e_0 b_w}{\gamma_r^2} , \quad (15)$$

$$\tau = \Omega_s z , \quad (16)$$

$$\alpha = 2k_\beta / \Omega_s , \quad (17)$$

$$\beta = k_s r_\beta^2 \alpha^2 / 4R , \quad (18)$$

$$\lambda = r_\beta^2 / 2w^2 . \quad (19)$$

Here, Ω_s defined by Eq. (15) is the synchrotron frequency averaged over a linear betatron orbit, β is the amplitude of the phase-front-curvature forcing term, and λ measures the spatial variation of field strength e_s within a betatron orbit. After substitution of (7) into (14) with the arbitrary choice of $\varphi_\beta = \pi/2$, we find

$$\frac{d^2\psi}{d\tau^2} = -e^{-\lambda \cos(\alpha\tau)} \sin\psi + \beta \cos(\alpha\tau) , \quad (20)$$

precisely the equation obtained by Rosenbluth.²

Resonance between the natural synchrotron oscillations and the periodic forcing occurs for $\alpha \approx 1$. Near resonance, values of β or λ above an α -dependent minimum will lead to rapid electron detrapping. In Sec. III we determine the

boundary for detrapping in (α, λ) space, with β set equal to the maximum value possible for a Gaussian vacuum beam.

III. DETRAPPING BOUNDARIES

Whether or not an electron whose motion is described by Eq. (20) is detrapped depends upon the three parameters α , β , and λ . The three parameters are not completely independent, however. For a vacuum Gaussian beam with waist radius w_0 , and for a given r_β ,

$$\beta = \frac{\alpha^2 r_\beta^2}{2w_0^2} \frac{z/z_R}{1+(z/z_R)^2}. \quad (21)$$

Thus β has a maximum at $z = z_R$:

$$\beta_{\max} = \frac{\alpha^2 r_\beta^2}{4w_0^2}. \quad (22)$$

Detrapping is strongest at (or very near) β_{\max} , where, since $w^2 = w_0^2 [1 + (z/z_R)^2]$,

$$\lambda = \frac{r_\beta^2}{2w^2} \equiv \frac{r_\beta^2}{4w_0^2}. \quad (23)$$

Thus, at the point of maximum detrapping in a given beam, α , β , and λ are related by

$$\beta_{\max} = \alpha^2 \lambda. \quad (24)$$

The boundary between trapped and detrapped orbits can therefore be reduced to a curve in α, λ space, with β at each point on the curve having the value given by Eq. (24).

Figure 1 is an approximate graph of that boundary

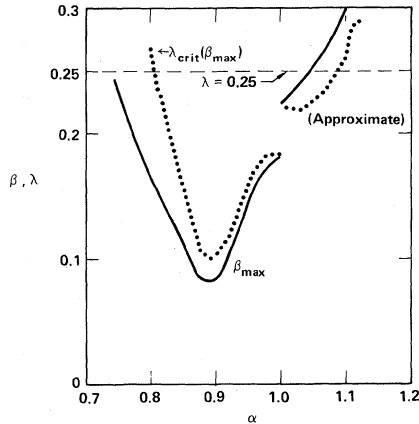


FIG. 1. Approximate boundary between trapped and resonantly detrapped single-particle orbits. Orbits described by Eq. (20) were numerically determined for a range of $\alpha \equiv 2k_\beta/\Omega_s$ and $\lambda \equiv r_\beta^2/2w^2$. For each (α, λ) point, β was assumed to have the maximum value possible ($\beta_{\max} = \alpha^2 \lambda$) for a vacuum Gaussian beam. The solid curve is β_{\max} versus α ; the dotted curve is λ_{crit} versus α . For a well-matched laser beam with $w_0^2 \approx r_\beta^2$, $\lambda = 0.25$ at $z = z_R$. Resonant detrapping can be important for the range of α between the two intersections of the dashed line $\lambda = 0.25$ and the dotted curve λ_{crit} , $0.8 \leq \alpha \leq 1.1$. The apparent discontinuity in the solid and dotted curves at $\alpha \approx 1$ is a reflection of the band structure for trapped orbits described in the text.

$\lambda_{\text{crit}}(\alpha)$. Particles whose orbits are characterized by $\lambda \geq \lambda_{\text{crit}}$ become detrapped. (The γ dependence of the synchrotron and betatron periods, for orbits with large γ - ψ variations, slightly raises the boundary shown in Fig. 1.) We have determined the curve by numerical integration of Eq. (20) with the initial conditions $\psi = d\psi/d\tau = 0$, so the boundary refers to detrapping from the bottom of the potential well. Our trapping criterion is that ψ remain less than π for $\tau \leq 100\pi$. Also plotted in Fig. 1 are the values of β_{\max} corresponding to λ on the detrapping boundary—so the figure may be considered a plot of the detrapping boundary in either α, λ or α, β space.

The boundary shown in the graph is only approximate because the location of trapped orbits on the plot is much more complicated than a simple boundary: Some orbits well above the curve remain trapped beyond $\tau = 1000\pi$. Trapped orbits appear to lie in bands on the diagram: The disappearance of trapping bands produces apparent discontinuities in the diagram, but the band locations depend strongly on the chosen trapping criterion. A more careful study of the trapping bands, with a more exact delineation of the detrapping boundary, is not relevant for the purposes of this paper, and we do not pursue the orbit structure further.

For an electron-beam radius $r_b \approx w_0$, $\lambda = 0.25$ at $z = z_R$, and β will remain less than $\alpha^2/4$ for most of the electrons. Figure 1 includes the line $\lambda = 0.25$; the range of α ($0.8 \leq \alpha \leq 1.1$) for which the detrapping boundary goes below that line is the range for which detrapping may be important.

Substitution for k_β and Ω_s in the definition of α gives the simple relation

$$\alpha = \xi (b_w/e_s)^{1/2}, \quad (25)$$

where the parameter ξ depends on the wiggler geometry; it is unity for a helical wiggler and $\sqrt{2}$ for a linear wiggler. (The difference is entirely in the expression for the betatron wave number, as long as rms values are used for b_w and e_s in the linear wiggler.) For betatron orbits of arbitrary eccentricity, α should be considered a function of radius through the radial variation in e_s . For a Gaussian laser profile with power P_l (in W),

$$\alpha(r) = 180 \xi e^{r^2/2w^2} \left[\frac{b_w^2 w^2}{P_l} \right]^{1/4}. \quad (26)$$

With reasonable assumptions about the parameters for an amplifier, α can be related more closely to laser power. For example, choosing $k_w w_0 = \frac{1}{3}$ and $a_w = z/z_R = 1$ gives

$$\alpha \approx 0.7 \xi [P_l (\text{GW})]^{-1/4} \quad (27)$$

on axis.

The range in α for which detrapping is important (0.8–1.1) translates to a laser-power range of $0.6 \leq P_l \leq 2.3$ GW for a linear wiggler, or $0.2 \leq P_l \leq 0.6$ GW for a helical wiggler. Taken at face value, these results suggest that FEL experiments must carefully avoid this power range or suffer great loss in trapping and energy-extraction efficiency. Presently, there is wide interest in amplifier designs which will start with initial

laser powers in the sub-GW—to-GW range and which would traverse this “danger” zone. The detrapping resonance is thus of practical interest.

In a tapered wiggler amplifier, however, both the wiggler taper (k_β decreasing with z) and the laser gain (Ω_s increasing with z) work to decrease α . Furthermore, gain rapidly straightens the phase fronts of a diverging laser field, decreasing β . All these effects conspire in the same way: to encourage electrons to move through resonance rapidly and safely (see Secs. IV and V).

Even in the absence of gain and taper, at least one other effect inhibits detrapping: a finite number of betatron wavelengths are required for a particle to detrap. To estimate roughly the distance required for detrapping, we can model Eq. (20) by the simpler expression

$$\frac{d^2\psi}{d\tau^2} = -\psi + \beta \cos\tau, \quad (28)$$

whose solution is

$$\psi(\tau) = \frac{\beta\tau}{2} \sin\tau + C_1 \sin\tau + C_2 \cos\tau. \quad (29)$$

A particle initially at rest in the bottom of the potential well ($C_1 = C_2 = 0$) will detrap when its maximum $\psi \approx \pi$. This occurs in a time $\tau(\psi = \pi) \approx 2\pi/\beta$. When $\alpha = 1$, $r_\beta = w_0$, and $\beta_{\max} = 0.25$, we find

$$k_\beta z(\psi = \pi) \approx 4\pi. \quad (30)$$

However, $\beta \approx \beta_{\max}$ only for of the order of one Rayleigh range [see Eq. (21)]. Using the definition of k_β and z_R , and the resonance relation (13), we find

$$k_\beta z_R = \frac{\gamma(k_w^2 w_0^2) a_w}{\sqrt{2}(1+a_w^2)} > 4\pi \quad (31)$$

for detrapping. Choosing, as before, $k_w w_0 \approx \frac{1}{3}$, evaluation of Eq. (31) at its peak of $a_w = 1$ indicates that a minimum γ is necessary for substantial detrapping in one Rayleigh range:

$$k_\beta z_R = 4\pi(\gamma/320). \quad (32)$$

However, if one insists that the half-height $\Delta\gamma_{1/2}$ of the ponderomotive well,⁴

$$\Delta\gamma_{1/2}(\text{bucket}) = \left[\frac{e_s b_w}{k_w^2} \right]^{1/2} = \frac{a_w}{\alpha}, \quad (33)$$

be approximately equal to the effective energy spread due to random transverse betatron motion (see Ref. 6),

$$\Delta\gamma_{1/2}(\text{transverse}) \approx \frac{\gamma(k_w^2 w_0^2) a_w^2}{4(1+a_w^2)}, \quad (34)$$

in order that a significant fraction of the particles be trapped, then relation (31) may be rewritten as

$$k_\beta z_R = \frac{2\sqrt{2}}{\alpha} \frac{\Delta\gamma_{1/2}(\text{transverse})}{\Delta\gamma_{1/2}(\text{bucket})}. \quad (35)$$

One sees that, for a well-designed wiggler [$\Delta\gamma_{1/2}(\text{bucket}) \geq \Delta\gamma_{1/2}(\text{transverse})$], a particle will spend less than a betatron wavelength in the resonant detrapping

region ($0.8 \leq \alpha \leq 1.1$) with β close to β_{\max} . To summarize these arguments, in order *purposely* to cause significant detrapping, one must choose relatively large values of both γ and $k_w w_0$ [relation (31)], low gain, and a very low initial trapping fraction [relation (35)]. Thus it is our opinion that designers of moderate- and high-gain FEL amplifiers should easily be able to avoid substantial detrapping from the betatron-synchrotron resonance, even near the critical power of 1 GW. These opinions are reinforced by the numerical simulations described in Secs. IV and V.

IV. A FREE-ELECTRON-LASER—SIMULATION CODE IN TWO DIMENSIONS

In order to avoid the restrictive assumptions required for the analytic theory, we have extensively modified a computer code⁷ to simulate numerically the effect of synchrotron-betatron resonance on a high-gain amplifier. The code models the interaction of an axisymmetric laser beam with an axisymmetric electron beam in a helical wiggler. A single ponderomotive potential well is followed in z , as in the codes described in Ref. 4. The propagation of radiation is described by the paraxial approximation,⁸ solved numerically with a finite-element method on a radial grid with generally ~ 60 grid points between the axis and $r_{\max} \geq 10w_0$. The electron-beam source for the radiation field is modeled by particles which move in straight-line orbits (constant r). These particles move in γ, ψ space according to Eqs. (5) and (6), but with $\gamma^2 \beta_1^2$ held constant. We have found that 256 particles at each of approximately 30 radial points provide more than sufficient accuracy for calculating the laser-field-source⁷ terms. We use a predictor-corrector method of the type developed by Gear⁹ to advance the field and particle equations simultaneously.

The code can design its own tapered wiggler; we have chosen to taper a_w with k_w held constant. The self-design is accomplished by maintaining a fictitious particle in a fixed circular betatron orbit (at $r = r_{\text{design}}$) at a constant positive $\psi = \psi_r$. As the particle decelerates [$d\gamma/dz < 0$, cf. Eq. (6)], the value of a_w is decreased to keep ψ constant for this single particle. This procedure may not lead to the optimum design,^{1,4} but suffices for the purposes of this paper.

The particles that move in straight-line orbits cannot exhibit the synchrotron-betatron resonance, of course; they do not undergo betatron motion. To study the resonance, we have added “test” particles which do undergo betatron motion as described by Eq. (1), while being decelerated in the laser field amplified by the straight-line particles. The physics of resonant detrapping is completely described by the test particles; their motion in γ, ψ space should unambiguously indicate the importance of detrapping in the presence of wiggler taper and gain.

A typical computer run follows 4096 test particles that are loaded with an equilibrium Gaussian distribution in x , y , v_x , and v_y . The code diagnostics examine these particles statistically. Nine other “probe” test particles are initialized (see below) with specific betatron orbits and locations in γ, ψ space: The orbits of these nine particles are

plotted as a diagnostic to permit a careful study of detraping effects seen only statistically in the majority of the particles.

Both sets of particles experience the off-axis effects of an increasing a_w [Eq. (3)] and changing laser field. In addition, the test particles naturally have a spread in $\gamma^2\beta_1^2$ at any given radius, just due to their betatron motion. In order to achieve consistency in energy loss between the straight-line and the test particles, an artificial spread in γ is introduced into the former. This spread represents the "equivalent energy spread" due to random transverse motion discussed in Ref. 6. (The other component of the overall energy spread described in Ref. 6 is due to the finite size of the electron beam in a wiggler field that increases off axis. This effect is naturally in the code.)

The code has an extensive set of diagnostic plots. The ones relevant to resonant detraping are as follows:

- (a) the power in the laser field as a function of z ;
- (b) the laser power calculated from conservation of laser-plus-test-particle power—this must approximately agree with the calculated laser power if the run is self-consistent (i.e., the initial spread in γ is properly chosen);
- (c) histograms of particle number versus final γ for both test and straight-line particles;
- (d) contours of φ (phase of electric field) in r and z ;
- (e) a plot of α versus z at several radii;
- (f) the γ - ψ orbits of the nine special test particles mentioned above.

These nine test particles are initialized in betatron orbits with a rms radius of r_{design} : three in linear orbits, three in elliptical, and three in circular orbits. In each set of three, ψ is set to $\psi_r, \psi_r \pm \pi/4$. All are started with $\gamma = \gamma_r$.

The particles in circular orbits do not "see" any phase-front curvature, and so should not be affected by the betatron-synchrotron resonance. The particles in linear orbits should be most strongly affected. The particle at $\psi = \psi_r$ in a circular betatron orbit should, by design, remain at $\psi = \psi_r$ in the self-designed taper, *except* for the fact that the fictitious design particle is kept at a fixed radius, while the betatron orbit of the test particle expands as a_w decreases.

V. SIMULATION-CODE RESULTS

We now discuss the results from a series of simulation runs centered at two electron-beam energies: $\gamma = 500$ and 100. The higher energy was chosen in order that the product $k_\beta z_R$ would be sufficiently large to cause significant detraping in the absence of any gain effects [see expressions (30) and (31)]. The lower energy was chosen in order that the ponderomotive potential well would be sufficiently deep to capture a large fraction of the electrons [see expressions (33) and (34)]. All runs had the following parameters in common:

$$a_w(z=0) = 1$$

$$\lambda_w = 8 \text{ cm (wiggler wavelength)},$$

$$r_b = w_0 = 0.424 \text{ cm } (k_w w_0 = \frac{1}{3}),$$

$$r_{\text{design}} = 0.707 r_b,$$

$$\psi_r = 0.35.$$

A. High-energy results

The choice of $\gamma = 500$ and the above parameters results in the laser wavelength $\lambda_s = 0.32 \mu\text{m}$ and $k_\beta z_R \approx 6.25\pi$. In our first run, the electron-beam current was made vanishingly small in order to isolate resonance detraping from any laser-gain effects over the propagation distance of $1.25z_R$. The laser-beam focus was $0.5z_R$ upstream of the wiggler. The laser intensity of 0.6 GW yielded $\alpha \approx 0.9$ (see Fig. 2), when $\beta \approx \beta_{\text{max}}$ at one Rayleigh range downstream of the laser focus, and an e_s such that $\Delta\gamma_{1/2}(\text{bucket})/\Delta\gamma_{1/2}(\text{transverse}) \approx 0.15$. The phase space trajectories of the nine special probe particles plotted in Fig. 3 show that five out of the six in elliptical and linear betatron orbits detrapped. The trajectories show an approximately linear increase of the ψ turning-point values with decreasing γ , symptomatic of what is expected from the resonance instability [see Eqs. (20) and (29)]. The sixth probe particle (upper right-hand corner of Fig. 3) initially shows large growth in its ψ excursions, but then apparently gets out of phase with the resonant driving term, and the excursions decrease rapidly during the last third of the run. We have seen similar effects in our numerical integrations of Eq. (20), probably due to the ψ dependence of the synchrotron frequency.

The spread in γ used for the straight-line particles in all of these runs was the effective energy spread due to betatron motion, Eq. (34). The difference between the final trapping fractions for the straight-line and test particles is therefore a fairly good indication of the importance of resonant detraping. Even in this first run, the difference is small ($\approx 5\%$ for the straight-line particles versus $\approx 4\%$ for the test particles; cf. Table I). We conclude that although detraping is unquestionably occurring here, its net effect is not large.

We increased the current in our second high-energy run to 1.0 kA. This led to a laser gain of $\approx 50\%$, as measured

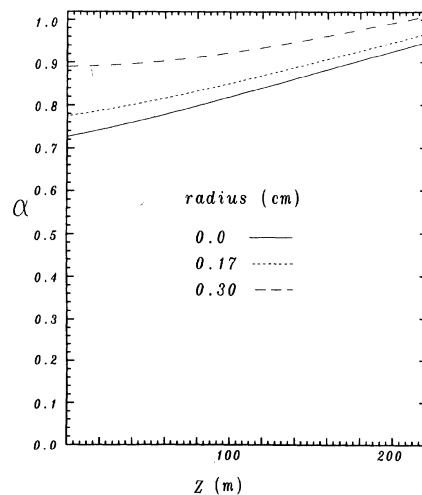


FIG. 2. Plot of the resonance parameter α versus z at three radii for a high-energy computer run ($\gamma = 500$, $a_w = 1$, $\lambda_w = 8$ cm, $\lambda_s = 0.32 \mu\text{m}$, $w_0 = r_b = 0.424$ cm, $r_{\text{design}} = 0.30$ cm, and $\psi_r = 0.35$) with infinitesimal electron-beam current. The z length of 221 m corresponds to 1.25 Rayleigh ranges.

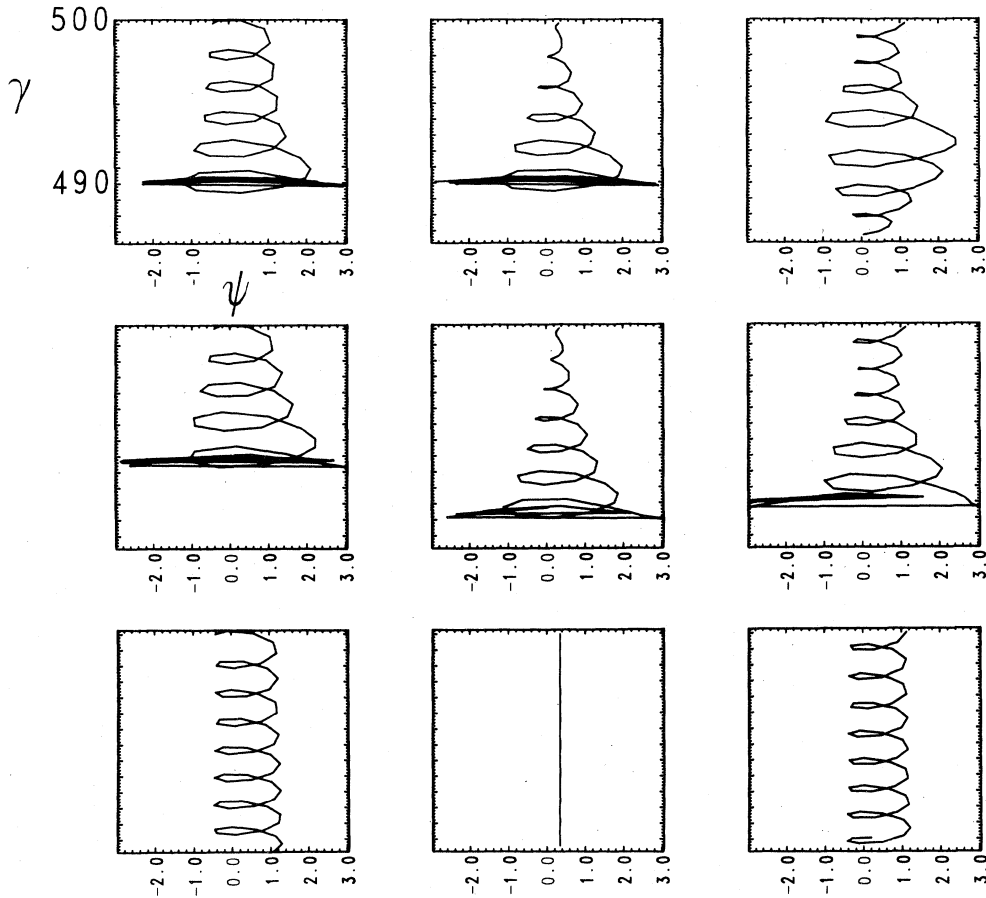


FIG. 3. Phase-space trajectories for the nine special test particles in the diverging laser field of Fig. 2. The abscissa is the particle's phase ψ modulo 2π . Detrapping is indicated by large excursions in ψ with little change in γ . The particles in the top row have linear betatron orbits, those in the middle, elliptical, and those in the bottom, circular. The three columns correspond to $\psi(z=0) = \psi_r - \pi/4$, ψ_r , and $\psi_r + \pi/4$. All but one of the particles in elliptical and linear orbits are resonantly detrapped by the phase-front curvature.

by the energy loss of both the straight-line and the test particles (see Fig. 4). None of the special probe particles detrapped as shown in Fig. 5, and comparison of the final cumulative histograms for the two sets of particles shows similar trapping fractions of 6% for each (see Table I).

In our last high-energy run, the current was again negligible (i.e., no laser gain), but the laser power was increased fourfold to 2.4 GW to increase the bucket height and decrease α by a factor of $\sqrt{2}$. The plot of the nine probe-particle trajectories in Fig. 6 now shows that none were

TABLE I. Trapping fractions.

γ	I_B (kA)	P_l (GW)	Percentage trapped	
			Straight line	Test
500	2.5×10^{-9}	0.6	5	4
500	1.0	0.6	6	6
500	2.5×10^{-9}	2.4	7	7
100	2.5×10^{-9}	0.6	22	25
100	1.0	0.6	23	26
100 ^a	2.5	0.4	22	23

^aFor this last run, the vacuum laser waist was $1.0z_R$ rather than $0.5z_R$ upstream of the wiggler entrance.

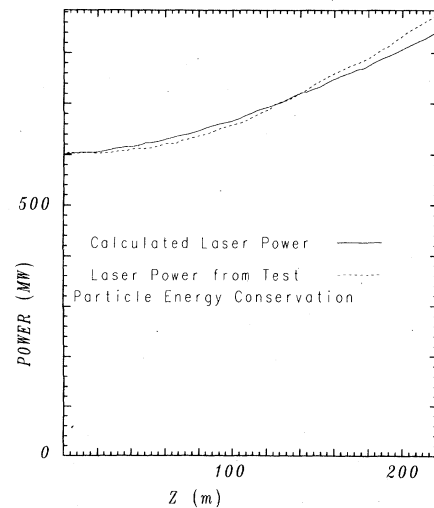


FIG. 4. Laser gain as measured by straight-line and test-particle energy loss for a high energy-run with the same parameters as in Fig. 2 except the electron-beam current is 1.0 kA. The similarity of the two energy-loss curves suggests that little resonant detrapping occurred in this instance.

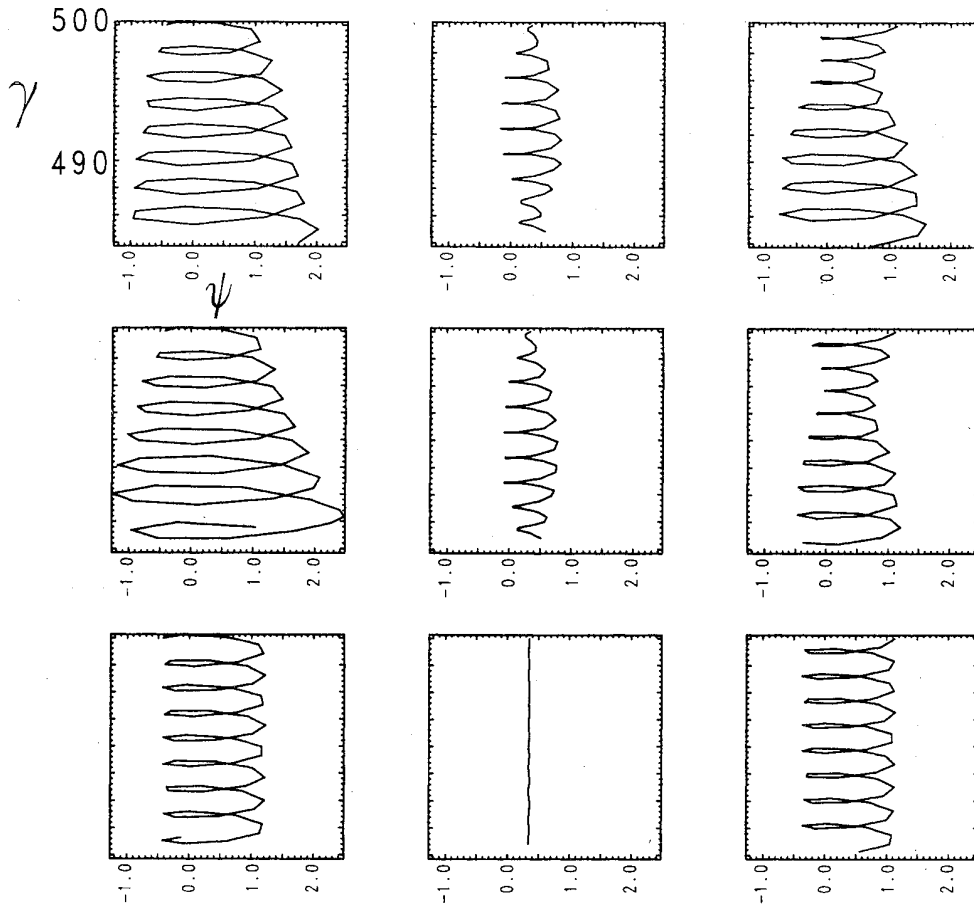


FIG. 5. Probe-particle trajectories for the run of Fig. 4. As compared with the no-gain run of Fig. 3, all of the probe particles remain trapped due to the laser gain reducing α .

detrapped and that essentially no growth in the ψ turning points occurred. The trapping fraction for both sets of particles was again very similar. We conclude that little detraping occurred in this run. These results imply that it is relatively easy at high energy to defeat the resonance instability by either increasing the initial laser intensity or obtaining sufficient energy extraction from the electron beam to cross the resonance region quickly.

B. Low-energy results

The low-energy computer runs had $\gamma = 100$, resulting in $\lambda_s = 8 \mu\text{m}$, $k_{\beta z_R} \approx 1.25\pi$, and $\Delta\gamma_{1/2}(\text{bucket}) / \Delta\gamma_{1/2}(\text{transverse}) \approx 0.8$.

The first run was one of no gain with a laser power of 0.6 GW and a vacuum waist $0.5z_R$ in front of the wiggler entrance. The probe particles show no detraping over the propagation distance of $2z_R$ (Fig. 7), although their ψ amplitude increased somewhat. The trapping fraction in both the test and straight-line particles was close to 25% (Table I), indicating that little or no detraping took place. The second low-energy run was identical to the first, except now the beam current was 1.0 kA. Again, no detraping was seen and the gain caused α to remain below 0.7 at r_{design} over most of the amplifier length.

In the last low-energy run, we decreased the initial laser power to 0.4 GW, increased the current to 2.5 kA, and put the laser focus one Rayleigh range upstream of the wiggler. These changes caused the value of α to remain in the resonant region for most of the propagation distance (Fig. 8). Nonetheless, none of the probe test particles detrapped and the final laser power (2.2 GW) from the straight-line particles is in good agreement with that (2.4 GW) extracted from the test particles. A glance at the r - z contours of the laser-field phase φ in Fig. 9 explains the lack of detraping. The strong laser gain led to a rapid straightening of the phase contours, effectively decreasing the magnitude of β by over a factor of 2, and preventing significant growth in the ψ turning points of the test particles.

In theory, a system with extremely high gain on axis can have a large, negative phase-front curvature which might persist for many Rayleigh ranges. However, for reasonable electron-beam currents (≤ 20 kA), we were unable to keep both negative phase curvature and α in the resonant region [i.e., $P_l(r \leq r_b) \sim 1$ GW], even with an initially converging laser beam. We believe it unlikely, then, that the resonant detraping instability can play an important role in FEL's for electron-beam energies in the 50-MeV region.

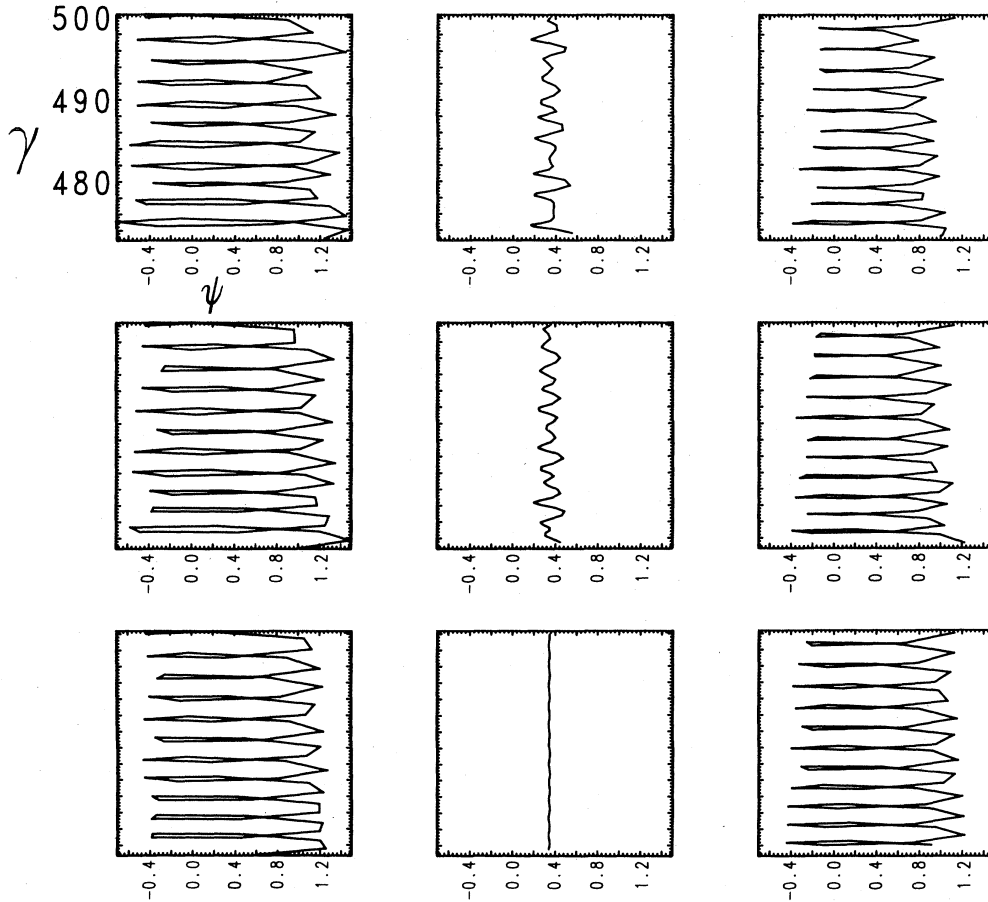


FIG. 6. Same as Fig. 3, except the laser power has been increased to 2.4 GW from 0.6 GW, thus reducing α by a factor of $\sqrt{2}$. No resonant detrapping is evident.

VI. DETRAPPING IN THE PRESENCE OF AN EXTERNAL FOCUSING FIELD

In the preceding sections we have considered betatron motion driven by the variation of a_w with r ; betatron motion due to additional focusing was explicitly neglected when the $d(a_w^2 + \gamma^2 \beta_1^2)/dz$ term in Eq. (12) was dropped. In the presence of external focusing, k_β is no longer given by Eq. (2), and $a_w^2 + \gamma^2 \beta_1^2$ is not constant on an electron's trajectory.

External focusing is likely to be used with a linear wiggler. The vector potential for a linear wiggler,

$$A = \sqrt{2} A_w \hat{x} \left[1 + \frac{k_w^2 y^2}{2} \right] \cos(k_w z), \quad (36)$$

results in betatron focusing in the y direction with

$$k_\beta = b_w / \gamma, \quad (37)$$

but no focusing in the x direction. In order to constrain electron-beam expansion in x , external focusing such as that due to quadrupole magnets will be necessary. Denoting k_q as the focusing wave number in the x direction, we have

$$\frac{d^2 x}{dz^2} = -k_q^2 x, \quad (38)$$

$$\frac{d^2 y}{dz^2} = -(k_\beta^2 - k_q^2) y,$$

for the betatron motion of a particle in the combined quadrupolar and wiggler magnetic fields. The sum $a_w^2 + \gamma^2 \beta_1^2$ is then no longer constant when averaged over a wiggler period:

$$\begin{aligned} \langle a_w^2 + \gamma^2 \beta_1^2 \rangle &= a_w^2(0) + \gamma^2 k_\beta^2 y_\beta^2 \\ &\quad - \gamma^2 k_q^2 y_\beta^2 \cos^2[(k_\beta^2 - k_q^2)^{1/2} z + \varphi_y] \\ &\quad + \gamma^2 k_q^2 x_\beta^2 \cos^2(k_q z + \varphi_x), \end{aligned} \quad (39)$$

where x_β and y_β are the maximum amplitudes of motion in the transverse directions, and φ_x and φ_y are initial betatron-orbit phases. In addition to a possible curvature-driven resonance term in Eq. (14), there are now the terms

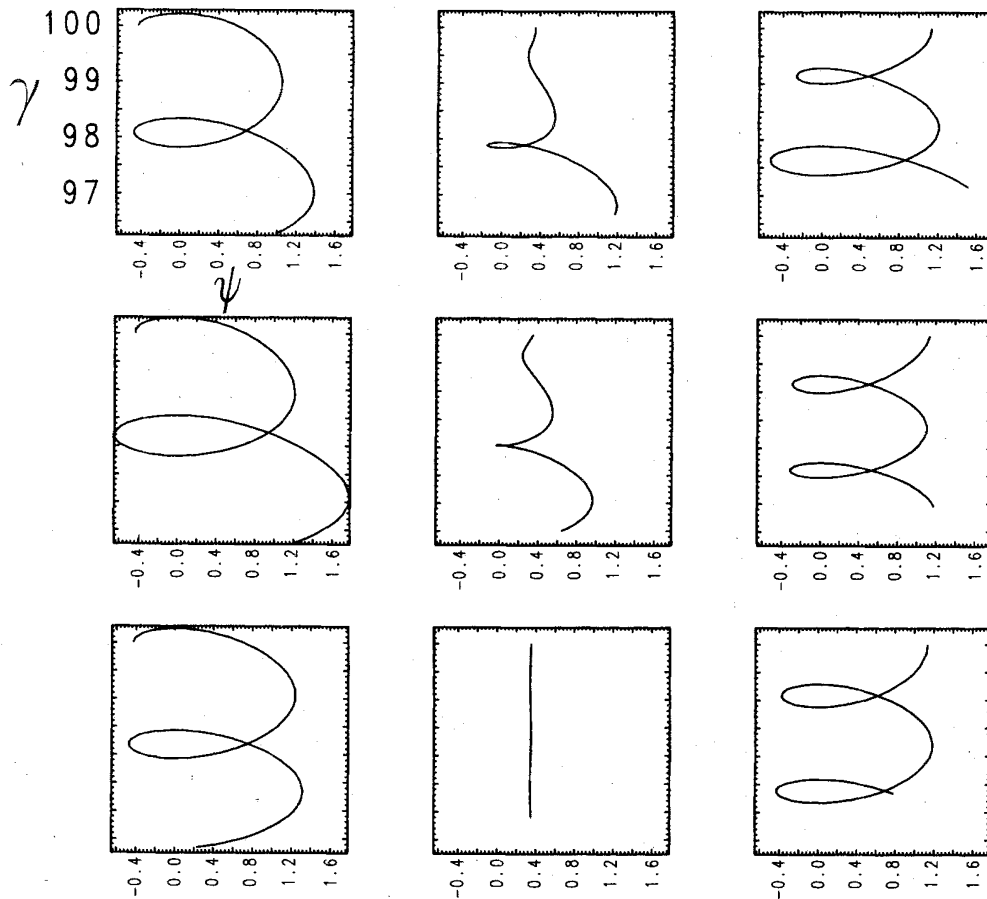


FIG. 7. Probe-particle trajectories in a low-energy ($\gamma=100$, $\lambda_s=8 \mu\text{m}$), no-laser-gain computer run. The total wiggler length was two Rayleigh ranges, but $k_{\beta z R} \approx 1.25\pi$ —only one-fifth as much as in the high-energy runs of Figs. 2–6.

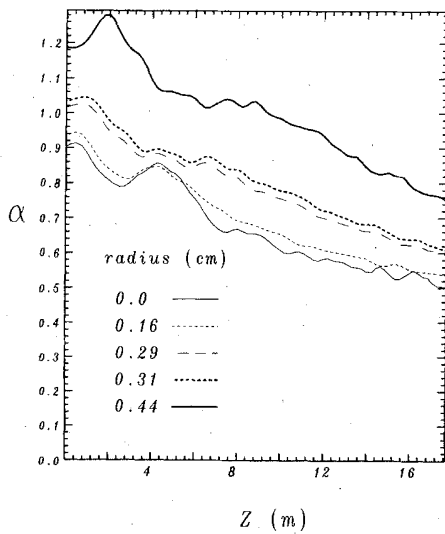


FIG. 8. Plot of α versus z for a low-energy run with initial laser power of 0.4 GW and a beam current of 2.5 kA. The laser gain was sufficient to offset diffraction and keep α in the de-trapping zone of $\approx 0.7-1.1$.

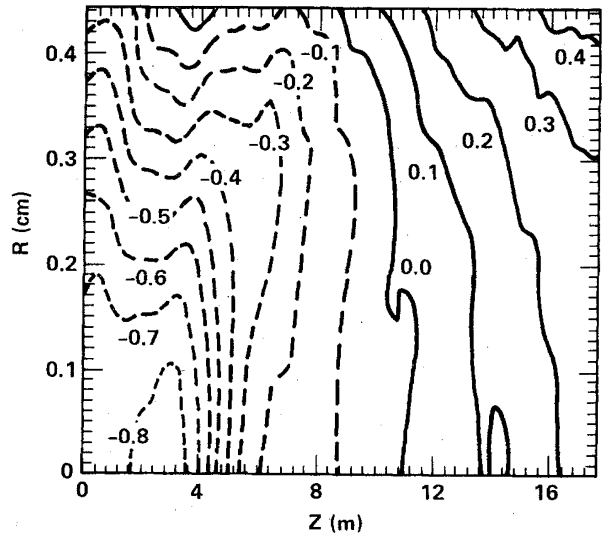


FIG. 9. r - z contour plot of the laser-field phase ϕ (in rad) corresponding to the computer run of Fig. 8. The initial laser beam had a vacuum waist one Rayleigh range in front of the wiggler entrance at $z=0$. The rapid laser gain in the first 4 m of propagation straightened the phase contours and significantly reduced the resonant driving term β , thus preventing serious de-trapping.

$$\begin{aligned} \frac{d^2\psi}{dz^2} = & -\Omega_s^2 \sin\psi + \cdots + \frac{k_s y_\beta^2}{2} k_q^2 (k_\beta^2 - k_q^2)^{1/2} \\ & \times \sin[2(k_\beta^2 - k_q^2)^{1/2} z + \varphi_y] \\ & - \frac{k_s x_\beta^2}{2} k_q^3 \sin(2k_q z + \varphi_x). \end{aligned} \quad (40)$$

For $k_q^2 \ll k_\beta^2$, Eq. (20) becomes

$$\frac{d^2\psi}{d\tau^2} \approx -e^{-\lambda \cos(\alpha\tau)} \sin\psi - k_{\beta z R} \frac{\alpha^2 k_q^2}{4k_\beta^2} \sin(\alpha\tau), \quad (41)$$

with $\alpha \equiv 2k_\beta/\Omega_s$. Negligible detrapping will occur if $\alpha < 0.5$ and the product

$$k_{\beta z R} \frac{k_q^2}{4k_\beta^2} \leq 1. \quad (42)$$

For this case of weak external focusing, however, the electron-beam shape will be highly elliptical if the initial emittance is the same in the x and y planes.

Another choice for external focusing would be to pick $k_q^2 = 0.5k_\beta^2$. The betatron oscillation periods in the x and y planes are then equal; thus, an initially circular electron beam will remain so when transported through the wiggler. Resonance now occurs when $\Omega_s = \sqrt{2}k_\beta$, and the relevant power levels for rapid detrapping are reduced by a factor of 4 from that found in Sec. III for curvature-driven detrapping. However, the magnitude of the driving term,

$$k_{\beta z R} (2k_\beta^2/\Omega_s^2)/2\sqrt{2}$$

for a circular orbit, can be much larger than the maximum possible, $\beta_{\max} \approx a^2/4$, in the curved-wave-front case [cf. Eq. (22)]. Even at high laser intensities with $\sqrt{2}k_\beta/\Omega_s \leq 0.5$ (i.e., far from the betatron-synchrotron resonance), detrapping may occur for large $k_{\beta z R}$. This is because the $a_w^2 + \gamma^2\beta_1^2$ variations along a betatron orbit cause γ_r [cf. Eq. (13)] to change too rapidly with z for the electron to follow in its synchrotron orbit.

The precise effect of external focusing depends on the details of the focusing, but strong external focusing in some cases can drive synchrotron-betatron detrapping more rapidly than can phase-front curvature. Phase-front

straightening from rapid gain will have no effect on this detrapping mechanism, so that external focusing is potentially much more dangerous than phase-front curvature.

VII. CONCLUSIONS

In this paper we have analyzed and simulated the resonant detrapping instability caused by the coupling between the synchrotron and betatron motions of electrons in a FEL amplifier. We have confirmed that Rosenbluth's² analysis applies in the laboratory frame and have investigated numerically the regions in parameter space where detrapping might be important. For reasonable choices of a_w and $k_w w_0$, the resonant region corresponds to a laser power of 0.2–0.6 GW for helical wigglers and 0.6–2.3 GW for linear wigglers (see Sec. III). However, because of the z dependence of the resonant driving term β , there is no electron-beam energy for which the critical laser energy is simultaneously sufficient to trap initially a reasonable percentage of the electrons, and for which detrapping will subsequently play an important role.

Runs with our two-dimensional simulation code confirm these conclusions, and also show that gain rapidly straightens the laser-field phase fronts and makes the electrons pass through the resonance region quickly. Taken together, all of these effects make it unlikely that FEL-amplifier experiments need encounter difficulty due to this detrapping resonance.

An initial analysis of the detrapping effects of external focusing suggests they may be large if such focusing is strong ($k_q/k_\beta \sim 1$) and $k_{\beta z R} \approx 1$. This detrapping will affect electrons in both highly elliptical and circular betatron orbits.

ACKNOWLEDGMENTS

We are pleased to acknowledge useful discussions with A. Sessler and M. Rosenbluth. This research was performed jointly under the auspices of the U. S. Department of Energy by Lawrence Livermore National Laboratory under Grant No. W-7405-ENG-48, and for the U. S. Department of Defense under the Defense Advance Research Projects Agency ARPA Order No. 4856, Program Code No. 3B10.

¹N. M. Kroll, P. L. Morton, and M. R. Rosenbluth, *IEEE J. Quantum Elec.* **QE-17**, 1436 (1981).

²M. N. Rosenbluth, Austin Research Associates Report No. ARA-488, 1983 (unpublished); for an alternative derivation, see C.-M. Tang and P. Sprangle, in *Free-Electron Generators of Coherent Radiation*, SPIE Volume 453, edited by C. A. Brau, S. F. Jacobs, and M. O. Scully (Society of Photo-Optical Instrumentation Engineers, Bellingham, Washington, 1983), p. 11.

³P. Diament, *Phys. Rev. A* **23**, 2537 (1981).

⁴D. Prosnitz, A. Szoke, and V. K. Neil, *Phys. Rev. A* **24**, 1436 (1981).

⁵W. B. Colson, *Phys. Lett.* **64A**, 190 (1977).

⁶C. A. Brau and R. K. Cooper, in *Physics of Quantum Electronics*, edited by S. F. Jacobs, C. T. Moore, H. S. Pilloff, M. Sargent, M. O. Scully, and R. Spitzer (Addison-Wesley, Reading, Mass., 1980), Vol. 7, p. 647.

⁷D. Prosnitz, R. A. Haas, S. Doss, and R. J. Gelinis, in *Physics of Quantum Electronics*, edited by S. F. Jacobs, C. T. Moore, H. S. Pilloff, M. Sargent, M. O. Scully, and R. Spitzer (Addison-Wesley, Reading, Mass., 1982), Vol. 9, p. 1047.

⁸J. H. Marburger, *Prog. Quantum Electron.* **4**, 35 (1975).

⁹C. W. Gear, *Commun. Ass. Comp. Mach.* **14**, 176 (1971).